Supporting Information

Gelinas et al. 10.1073/pnas.0909203106

SI Materials and Methods

Protein Expression and Purification. DNA encoding Stn1-C (amino acids 288–494) or Ten1 (amino acids 2–102) and an N-terminal thrombin cleavage site were cloned into the pETDUET (Novagen) vector and the proteins were expressed in BL21 (DE3) cells. Cells were lysed by sonication and the cleared lysate was passaged over a $NiCl_2$ Chelating Sepharose column (GE Healthcare), followed by washing and eluting of the Stn1-C or Ten1 protein. The N-terminal histidine tag was removed from the purified Stn1-C protein via incubation with Bovine Alpha Thrombin protease (Haematologic Technologies). After cleavage, thrombin activity was inhibited by the addition of biotinylated FPR-chloromethylketone (Haematologic Technologies). The Stn1-C protein was then further purified to homogeneity using a Superdex G200 column (GE Healthcare), and the peak corresponding to monomeric protein was pooled, concentrated and stored at −80 °C. After the $NiCl_2$ Chelating Sepharose column, the Ten1 protein was purified to homogeneity using a Superdex G75 column (GE Healthcare). Fractions corresponding to monomeric Ten1 were pooled and the N-terminal histidine tag was removed via incubation with Bovine Alpha Thrombin protease (Haematologic Technologies). After cleavage, thrombin activity was inhibited by the addition of biotinylated FPR-Chloromethylketone (Haematologic Technologies). Purified Ten1 protein was aliquoted and stored at −80 °C.

Crystallization and Data Collection. Initial crystallization conditions for Stn1-C were found using Crystal Screen I (Hampton Research) and the hanging drop vapor diffusion method. Stn1-C crystal growth conditions were optimized, the best growth resulting at 17 °C by mixing 4 μL of Stn1-C (5.8 mg/mL) with 4 μL of 0.1 M Tris·HCl, pH 8.4, 15% (wt/vol) PEG 1000, 10 mM EDTA. Maximum crystal growth was achieved after ≈7 days of incubation. Crystals were cryoprotected in the mother liquor solution supplemented with 20% glycerol and flash frozen in liquid nitrogen. Gold derivatives were made by soaking crystals in the mother liquor supplemented with 20% glycerol and 6 mM $KAuCl_4$ at 17 °C for 3 h followed by flash freezing in liquid nitrogen. The Native 1 crystals were soaked in $PtCl_4$; however, a difference Fourier transform map revealed no Pt occupancy. Au and native datasets were collected on the CuK_α rotating anode homesource X-ray beam. Subsequent data collection of native and $KAuCl_4$ soaked crystals was performed on beamline X29A of the National Synchrotron Light Source (Brookhaven National Laboratories).

Initial crystal conditions for the Ten1 protein were identified using the Phoenix automated drop setter (Art Robbins Instruments) (0.2 μL of protein: 0.2 μL of crystal condition, 50 μL well) and corresponded to the PEG Ion Screen (Hampton Research) condition 18 [0.2 M potassium nitrate 20% (wt/vol), PEG 3350]. Crystals were reproduced at 17 °C by mixing 2 μL protein (5.76 mg/mL) with 2 μL of 0.2 M potassium nitrate, 25% (wt/vol) PEG 3350. The crystal used for data collection was achieved via macroseeding into a new drop containing 2 μL of protein (5.76 mg/mL) mixed with 2 μL of 0.2 M potassium nitrate, 20% (wt/vol) PEG 3350. The iodine derivative was made by soaking a native crystal in a solution of 650 mM potassium iodide, 35% glycerol for 30 s followed by flash freezing in liquid nitrogen.

Experimental Phasing and Structure Refinement. The structure of Stn1-C was determined via SIRAS with an Au derivative crystal. Data processing and scaling for Native 1 and Au derivative datasets was performed with d*TREK via CrystalClear (Rigaku) with diffraction limits on the homesource CuK_α X-ray beam of 3.0 and 3.1 Å, respectively. The heavy atom substructure, initial phasing, and density modification were performed using SOLVE/RESOLVE as part of the PHENIX Crystallography Suite (1, 2). Data were processed in the space group $P4_12_12$, and two heavy atom sites were identified using AutoSol (1, 2). Calculation of initial phases and density modification using RESOLVE (2) yielded an electron density map with clear contiguous density. However, inspection of the helical segments revealed that they were the mirror image of an α helix comprised of L-amino acids, indicating that the space group was in fact $P4_32_12$. The data were reprocessed using the correct space group and three heavy atom sites were found [figure of merit (FOM) = 0.38] using AutoSol (1, 2). Density modification improved the FOM to 0.77. The resulting density modified experimental map (Fig. S1*A*) showed clear density for secondary structure. An initial model was then built using PHENIX AutoBuild (3) and resulted in a model containing 157 sequence assigned residues. The model obtained using PHENIX AutoBuild was used for molecular replacement with a higher resolution native dataset using CNS (4). Higher resolution synchrotron data (Native 2), 2.5 Å, was processed and scaled using HKL2000 (5). Electron density for the N-terminal 25 amino acids, residues 288–312 was missing, as well as electron density for 9 amino acids, residues 472–480, in a loop in the C-terminal region and two residues, 493–494, at the extreme C terminus. Rebuilding of side chains and modeling was completed using manual building with COOT (6). Several iterations of building and refinement, with CNS (4), were performed. Rigid body refinement, simulated annealing, energy minimization, and *B*-factor refinement were completed using CNS while monitoring the R_{work} and R_{free} values. Solvent molecules were added to the structure using water-picking in CNS. CNS model statistics reports a final R_{work} of 24.6 and R_{free} of 30.1 (Fig. S1*B*) with a cross-validated Luzzati coordinate error of 0.58 Å. MolProbity (7) was used for structure validation. The MolProbity Ramachandran analysis identifies 158 of 166 residues in favored regions, and 166 of 166 residues in allowed regions.

A complete single-wavelength anomalous dispersion (SAD) dataset was collected on the homesource CuK_α X-ray beam for Ten1. The collection strategy included continuous collection throughout the entire oscillation range. The images were indexed and integrated using MOSFLM (8, 9), scaled and averaged using SCALA (9, 10) under the H3 space group as advised by POINTLESS (9, 10). PHENIX Xtriage (1, 3) indicated anomalous signal up to 2.0 Å. PHENIX AutoSol was used to determine the iodide positions and calculate density modified experimental maps. A total of eight refined positions were found (FOM 0.56 and 0.74 before and after density modification, respectively), and the experimental density map showed clear features of the protein backbone and well defined side chains. Automated building with PHENIX AutoBuild resulted with a model containing 80 sequence assigned residues when refined against the experimental phases. The remaining 20 sequence assigned residues were manually built using COOT and refined against model phases in CNS via simulated annealing, energy minimization, and *B*-factor refinement while monitoring the R_{work} and R_{free} values. Solvent molecules were added to the structure using water-picking in CNS. CNS model statistics reports a final R_{work} of 18.8 and R_{free} of 23.8 with a cross-

validated Luzzati coordinate error of 0.27 Å. MolProbity was used for structure validation. The MolProbity Ramachandran analysis indicates all residues were in favored/allowed regions.

All reported superpositions were done using STRAP (12) and all structural figures were made using PyMOL (11). Solvent excluded surface areas of binding interfaces were determined as follows. For the Stn1-C interface, the solvent accessible surface area for the individual wHTH lobes (residues 313–397 and residues 398–491) was calculated in PyMOL (11). The solvent accessible surface area for the whole structure (residues 313–491) was also calculated in PyMOL and subtracted from the sum of the individual lobes. The electrostatic surface representations of the Stn1-C structure were made using the APBS tool in PyMOL and are shown with low and high potentials of −2 and + 2, respecitively (11). For the interface of the β-barrel with the C-terminal helix in Ten1, the solvent accessible surface area for the β-barrel (residues 3–83) and the loop and C-terminal helix (residues 84–101) were individually calculated in PyMOL. The solvent accessible surface area for the entire structure (residues 3–101) was also calculated in PyMOL and subtracted from the sum of the β-barrel, loop and C-terminal helix.

1. Zwart PH, et al. (2008) Automated structure solution with the PHENIX suite. *Methods Mol Biol* 426:419–435.
2. Terwilliger T (2004) SOLVE and RESOLVE: Automated structure solution, density modification and model building. *J Synchrotron Radiat* 11:49–52.
3. Terwilliger TC, et al. (2008) Iterative model building, structure refinement and density modification with PHENIX Autobuild wizard. *Acta Crystallogr D Biol Crystallogr* 64:61–69.
4. Brunger AT, et al. (1998) Crystallography & NMR system: A new software suite for macromolecular structure determination. *Acta Crystallogr D Biol Crystallogr* 54:905–921.
5. Otwinowski Z, Minor W (1997) Processing of x-ray diffraction data collected in oscillation mode. *Methods Enzymol* 276:307–326.
6. Emsley P, Cowtan K (2004) COOT: Model-building tools for molecular graphics. *Acta Crystallogr D Biol Crystallogr* 60:2126–2132.
7. Davis IW, et al. (2007) MolProbity: All-atom contacts and structure validation for proteins and nucleic acids. *Nucleic Acids Res* 35:W375–W383.
8. Project CCC (1994) The CCP4 suite: Programs for protein crystallography. *Acta Crystallogr D Biol Crystallogr D* 50:760–763.
9. Leslie AGW (1992) Recent changes to the Mosflm package for processing film and image plate data. *Joint CCP4 + ESF-EAMCB Newsletter on Protein Crystallography* No. 26.
10. Evans P (2006) Scaling and assessment of data quality. *Acta Crystallogr D Biol Crystallogr* 62:72–82.
11. DeLano W (2002) *The PyMOL User's Manual* (DeLano Scientific, San Carlos, CA).
12. Gille C, Frommel C (2001) STRAP: editor for STRuctural Aligments of Proteins. *Bioinformatics* 17:377–378.

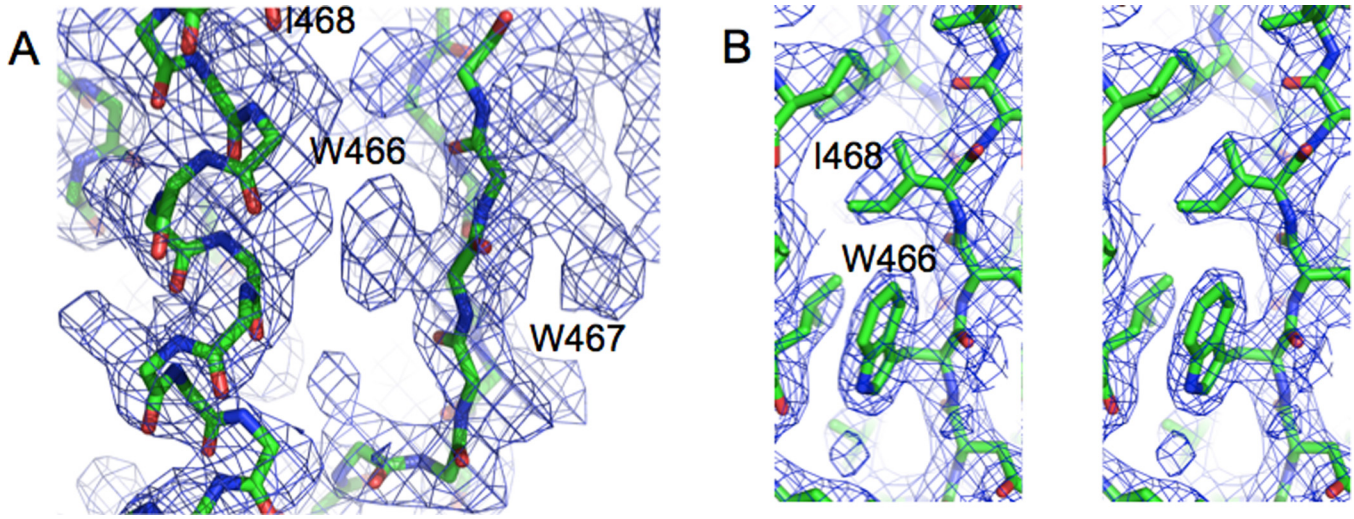

Fig. S1. Experimental and refined electron density maps for the Stn1-C structure determination. (*A*) Experimental electron density map at 3.1-Å resolution, contoured at 1 σ. Map obtained using SIRAS with a gold derivative crystal. The peptide backbone is clearly defined and density for the large tryptophan side chains is visible. (*B*) Stereoview of the refined electron density map for Stn1-C contoured at 1.0 σ.

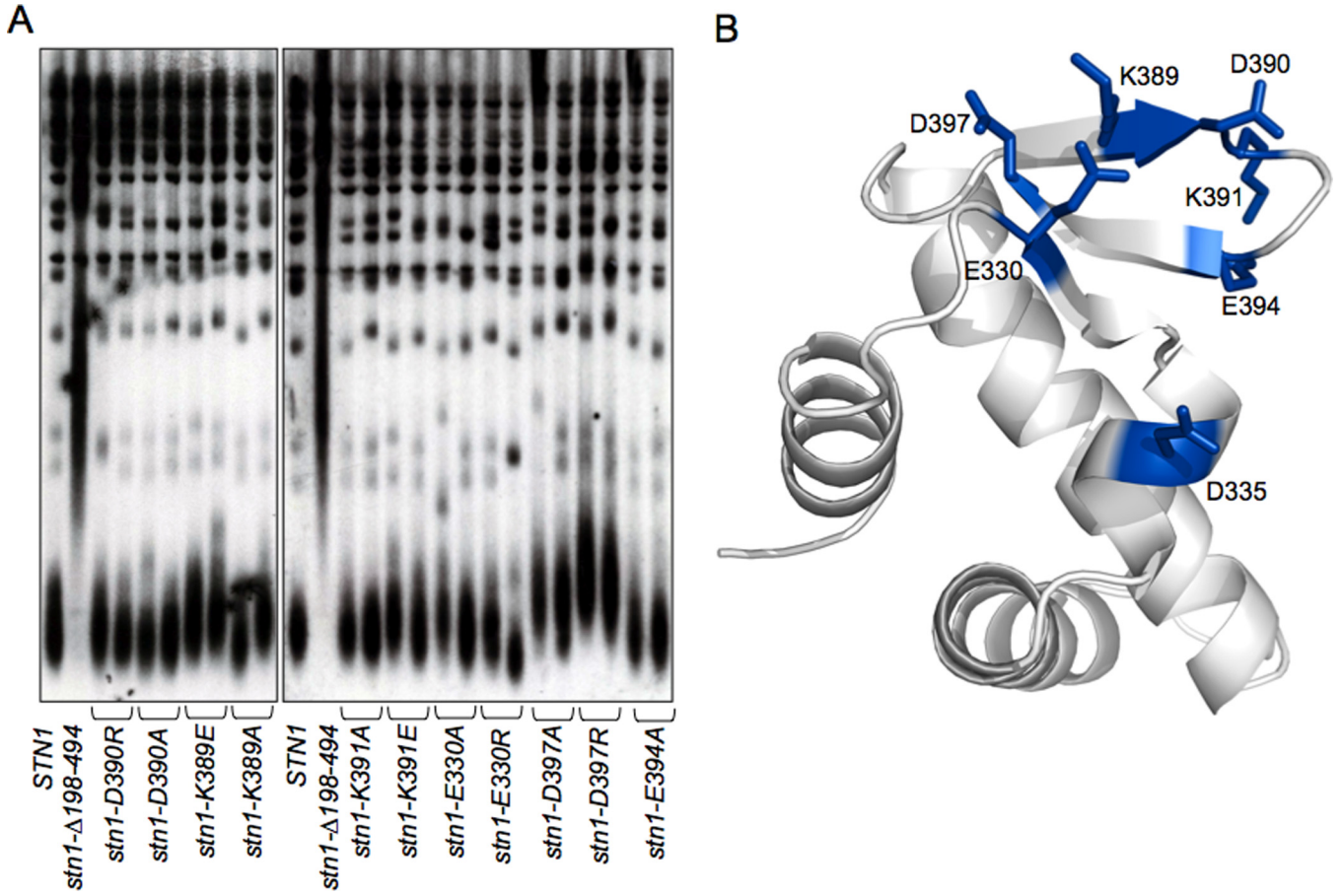

Fig. S2. Mutations in the N-terminal wHTH lobe of Stn1 do not affect telomere length. (*A*) Telomere length of strains expressing mutations introduced into the β-sheet region of the N-terminal domain. (*B*) Location of mutations tested on the N-terminal wHTH lobe of Stn1-C, with the C-terminal lobe removed for ease of viewing. Figure prepared using PyMOL (11).

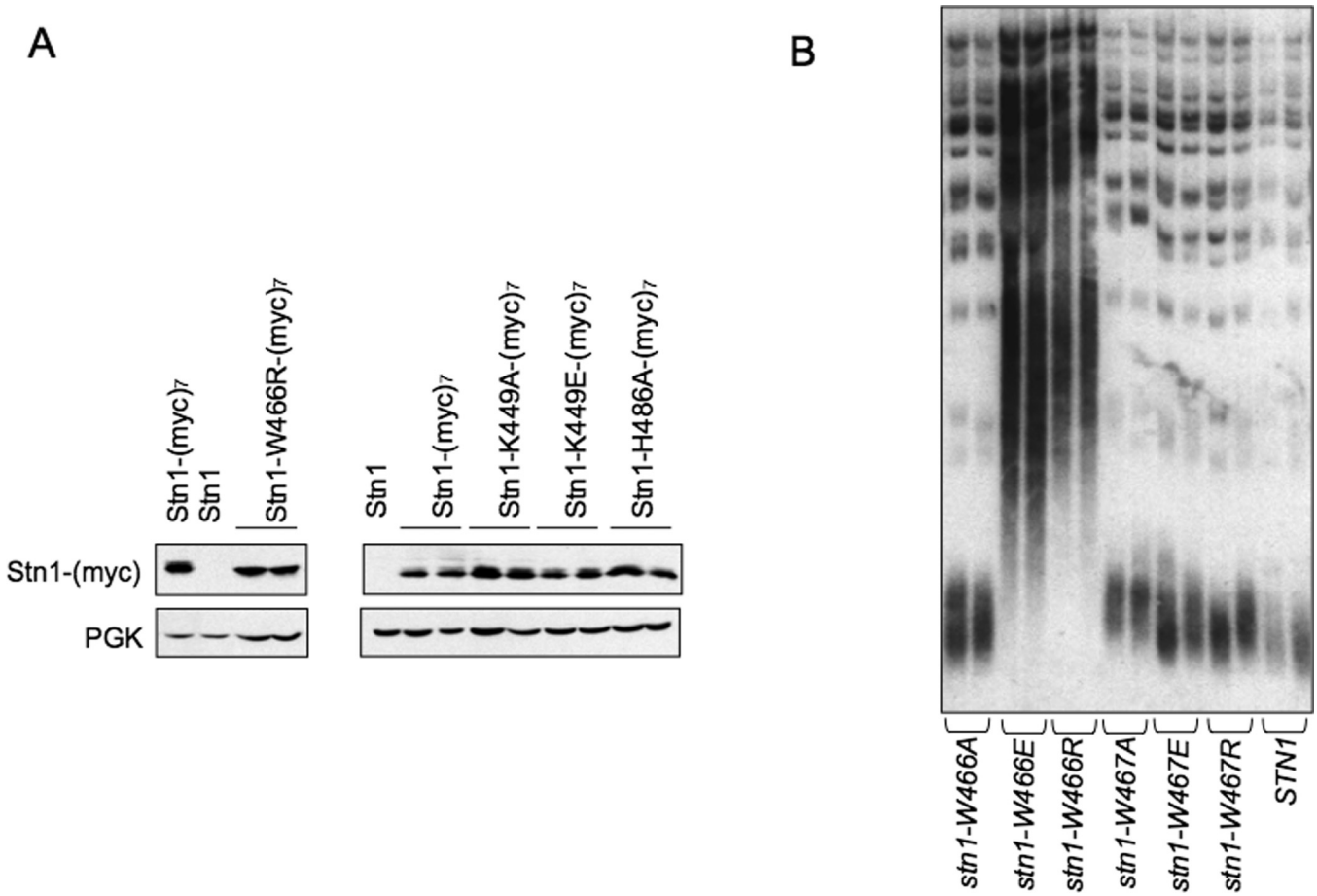

Fig. S3. Additional analysis of *stn1*-W466E and *stn1*-W466R. (*A*) Steady state protein levels of the Stn1-W466R mutant protein are indistinguishable from that of wild type; several other mutant alleles of Stn1 are also indicated. (*B*) Telomeres in the *stn1*-W466E and *stn1*-W466R strains exhibit pronounced elongation.

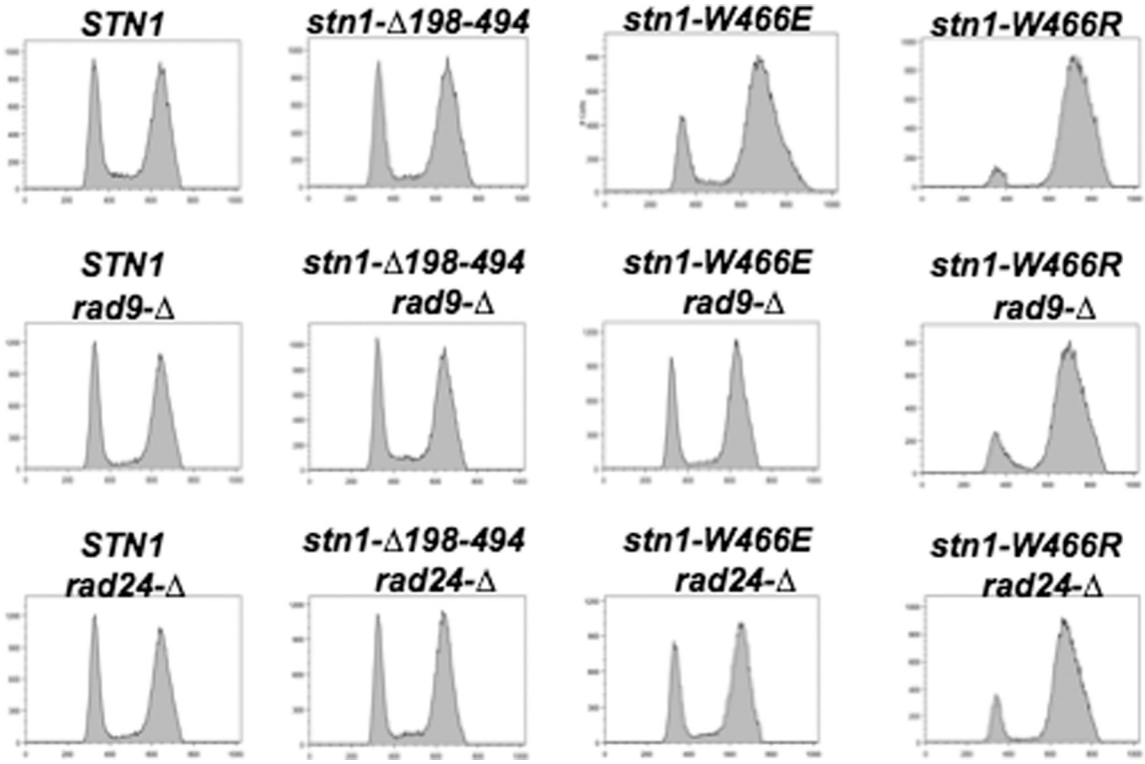

Fig. S4. Flow cytometry profile of log-phase cultures of the indicated strains, fixed and stained with SYTOX green; each graph represents data from 50,000 cells.

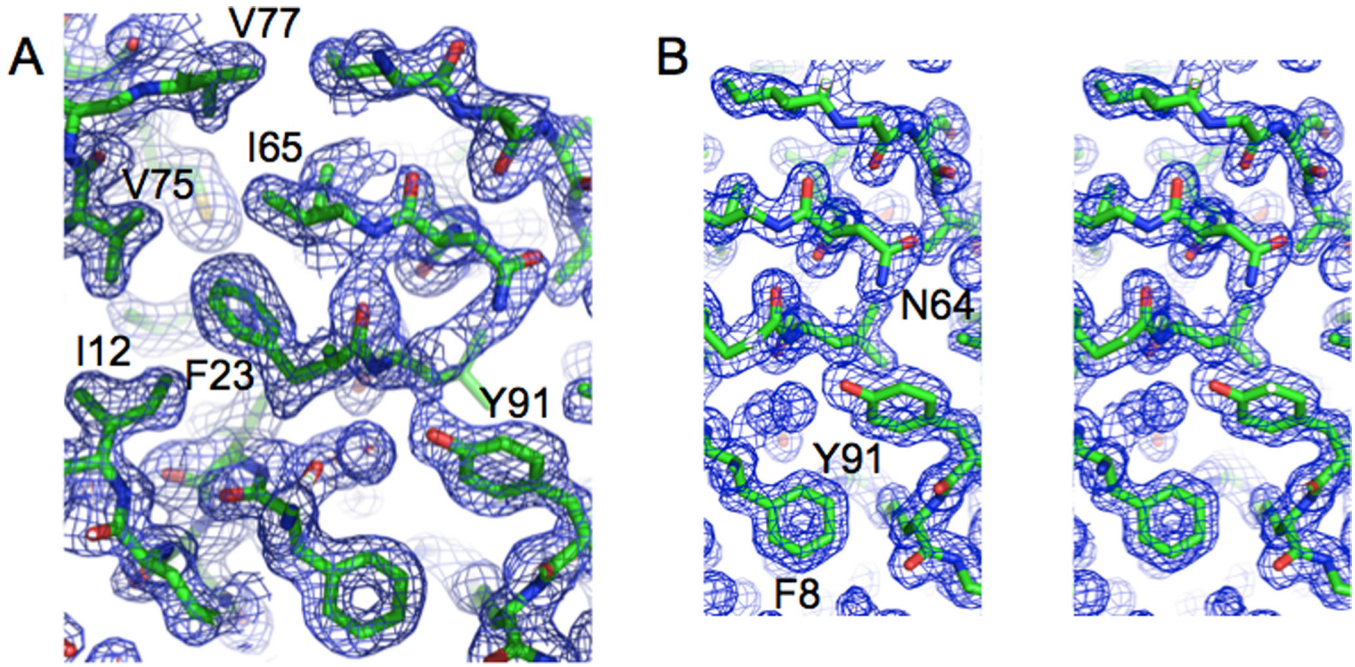

Fig. S5. Experimental and refined electron density maps for the Ten1 structure determination. (*A*) Experimental electron density map at 1.7-Å resolution, achieved via SAD with an iodide derivative crystal contoured at 1.0 σ. Clear electron density was visible for the peptide backbone as well as amino acid side chains, which are labeled. (*B*) Stereoview of the refined electron density map for Ten1 contoured at 1.0 σ.

Table S1. Data collection, phasing and refinement statistics for Stn1-C

	Native 1	Au derivative	Native 2
Data collection			
Space group	$P4_32_12$	$P4_32_12$	$P4_32_12$
Cell dimensions			
a, b, c; Å	52.8, 52.8, 187.2	52.8, 52.8, 168.8	52.7, 52.7, 186.6
α, β, γ; °	90.0, 90.0, 90.0	90.0, 90.0, 90.0	90.0, 90.0, 90.0
Resolution, Å	46.1–3.00 (3.11–3.00)	45.9–2.53 (2.62–2.53)	50.0–2.48 (2.59–2.48)
R_{sym} or R_{merge}	0.091 (0.238)	0.122 (0.287)	0.179 (0.423)
$I/\sigma I$	12.4 (5.6)	7.6 (2.4)	36.1 (3.7)
Completeness, %	98.7 (98.3)	98.4 (89.0)	94.8 (71.9)
Redundancy	3.83 (3.81)	3.26 (1.48)	8.7 (7.8)
Refinement			
Resolution, Å			20–2.5
No. reflections			10,710
R_{work}/R_{free}			0.246/0.301
No. atoms			
Protein			1,344
Water			146
B factors			
Protein			55.3
Water			47.1
rmsd			
Bond lengths, Å			0.0087
Bond angles, °			1.31
Ramachandran outliers			None
Luzzati cross-validated coordinate error, Å			0.58

Values in parentheses are for highest-resolution shell.

Table S2. Data collection, phasing and refinement statistics for Ten1

	Iodine derivative
Data collection	
Space group	*R*3
Cell dimensions	
a, *b*, *c*; Å	64.3, 64.3, 66.2
α, β, γ; °	90.0, 90.0, 120.0
Resolution, Å	25.7–1.70 (1.79–1.70)
R_{sym} or R_{merge}	0.048 (0.336)
$I/\sigma I$	16.2 (2.2)
Completeness, %	94.5 (94.5)
Redundancy	4.5 (2.7)
Refinement	
Resolution, Å	20–1.7
No. reflections	10,630
R_{work}/R_{free}	0.188/0.238
No. atoms	
Protein	774
Water	153
B factors	
Protein	24.2
Water	66.2
rmsd	
Bond lengths, Å	0.0207
Bond angles, °	2.02
Ramachandran outliers	None
Luzzati cross-validated coordinate error, Å	0.27

Values in parentheses are for highest-resolution shell.